Neuron
Article

Basal GABA Regulates $GABA_BR$ Conformation and Release Probability at Single Hippocampal Synapses

Tal Laviv,[1,3] Inbal Riven,[1,3,4] Iftach Dolev,[1] Irena Vertkin,[1] Bartosz Balana,[2] Paul A. Slesinger,[2] and Inna Slutsky[1,*]
[1]Department of Physiology and Pharmacology, Sackler Faculty of Medicine, Tel Aviv University, 69978 Tel Aviv, Israel
[2]Peptide Biology Laboratory, The Salk Institute for Biological Studies, 10010 North Torrey Pines Road, La Jolla, CA 92037, USA
[3]These authors contributed equally to this work
[4]Present address: Department of Chemical Physics, Weizmann Institute of Science, 76100 Rehovot, Israel
*Correspondence: islutsky@post.tau.ac.il
DOI 10.1016/j.neuron.2010.06.022

SUMMARY

Presynaptic $GABA_B$ receptor ($GABA_BR$) heterodimers are composed of GB_{1a}/GB_2 subunits and critically influence synaptic and cognitive functions. Here, we explored local $GABA_BR$ activation by integrating optical tools for monitoring receptor conformation and synaptic vesicle release at individual presynaptic boutons of hippocampal neurons. Utilizing fluorescence resonance energy transfer (FRET) spectroscopy, we detected a wide range of FRET values for CFP/YFP-tagged GB_{1a}/GB_2 receptors that negatively correlated with release probabilities at single synapses. High FRET of $GABA_BRs$ associated with low release probability. Notably, pharmacological manipulations that either reduced or increased basal receptor activation decreased intersynapse variability of GB_{1a}/GB_2 receptor conformation. Despite variability along axons, presynaptic $GABA_BR$ tone was dendrite specific, having a greater impact on synapses at highly innervated proximal branches. Prolonged neuronal inactivity reduced basal receptor activation, leading to homeostatic augmentation of release probability. Our findings suggest that local variations in basal GABA concentration are a major determinant of GB_{1a}/GB_2 conformational variability, which contributes to heterogeneity of neurotransmitter release at hippocampal synapses.

INTRODUCTION

Probability of neurotransmitter release (*Pr*) is a critical determinant of synaptic strength in neuronal connections. Presynaptic inhibition mediated via G protein-coupled receptors (GPCRs) constitutes a widespread, evolutionary conserved, regulatory root of neurotransmitter release (Wu and Saggau, 1997). Among diverse presynaptic GPCR types, $GABA_BRs$ are known to inhibit basal synaptic transmission in a wide range of central synapses. $GABA_BRs$ are obligatory heterodimers, requiring two homologous subunits, GB_1 and GB_2, for functional expression (Jones et al., 1998; Kaupmann et al., 1998; White et al., 1998). Molecular diversity of $GABA_BRs$ arises from two pharmacologically indistinguishable GB_1 isoforms, 1a and 1b (Bettler et al., 2004) that couple to the pertussis toxin-sensitive G proteins, G_i and G_o. Recent generation of isoform-specific GB_1 knockout mice revealed a critical role of GB_{1a}/GB_2 receptors, mainly localizing at presynaptic boutons, in regulation of long-term potentiation and hippocampus-dependent memory function (Vigot et al., 2006).

Although existence of $GABA_BR$ heterodimers as molecular entities has been recently accepted, physiological patterns of neuronal activity that induce local receptor activation at presynaptic boutons and, consequently, inhibition of neurotransmitter release, remain controversial. Electrophysiological studies in hippocampal slices provided conflicting observations, ranging from tonic inhibition of glutamate release mediated by $GABA_BRs$ during spontaneous synaptic activity (Jensen et al., 2003), to a necessity of high-level interneuron activity to activate presynaptic heteroreceptors (Isaacson et al., 1993). Conversely, only postsynaptic receptor activation was detected during pharmacologically induced rhythmic oscillations (Scanziani, 2000). These studies typically estimated average effects of endogenous GABA on neurotransmitter release over populations of synapses. Given a profound heterogeneity in release properties across hippocampal synapses (Branco et al., 2008; Dobrunz and Stevens, 1997; Murthy et al., 1997; Rosenmund et al., 1993; Slutsky et al., 2004), averaging might obscure the influence of local extracellular GABA concentration ($[GABA]_o$) at the single-synapse level.

In attempt to explore local $GABA_BR$ activation at individual presynaptic boutons, we integrated optical techniques for simultaneous monitoring of protein-protein interactions and synaptic vesicle recycling. Fluorescence resonance energy transfer (FRET) spectroscopy has been utilized to estimate intermolecular associations between CFP/YFP-tagged receptor subunits, whereas activity-dependent FM styryl dyes have been used to detect presynaptic activity at single hippocampal boutons. We have used this system to address the following questions: does basal GABA activate the GB_{1a}/GB_2 receptor and decrease synaptic vesicle release probability? If so, does this basal receptor activation vary across synapses, contributing to heterogeneity of presynaptic strength? Do presynaptic boutons adapt to chronic changes in ongoing neuronal activity by regulating the extent of basal $GABA_BR$ activation?

Our results reveal that basal synaptic activity promotes GB_{1a}/GB_2 association by a variable degree across boutons along

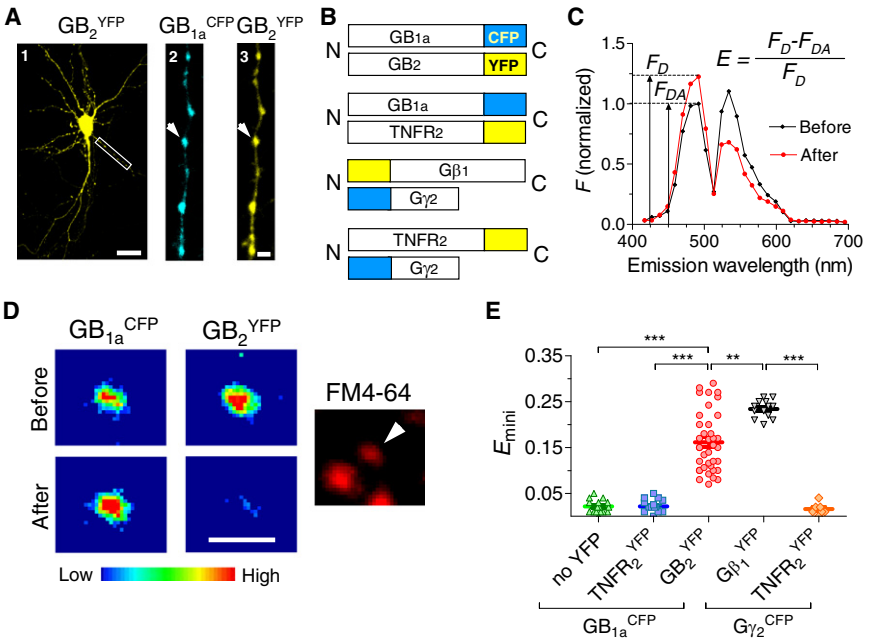

Figure 1. Monitoring GB$_{1a}$/GB$_2$ Interactions by FRET at Hippocampal Boutons

(A) Representative confocal images of pyramidal neuron in hippocampal culture that was cotransfected with GB$_2^{YFP}$ and GB$_{1a}^{CFP}$. White box in (A$_1$) corresponds to the blow-ups in (A$_2$) and (A$_3$). Arrowheads: the bouton that was bleached for calculation of FRET efficiency in (C) and (D).

(B) Schematic illustration of fusion protein constructs used for FRET detection: GB$_{1a}^{CFP}$/GB$_2^{YFP}$, GB$_{1a}^{CFP}$/TNFR$_2^{YFP}$, Gβ$_1^{N'\text{-}YFP}$/Gγ$_2^{N'\text{-}CFP}$, and TNFR$_2^{YFP}$/Gγ$_2^{N'\text{-}CFP}$.

(C) Detection of FRET efficiency (E) by spectral approach under 405 nm excitation in a single bouton. Donor emission pick before (F_{DA}) and after (F_D) photobleaching. E = 0.24.

(D) Pseudo-color coded fluorescent images of GB$_{1a}^{CFP}$ and GB$_2^{YFP}$ proteins expressed in a functional bouton before and after YFP photobleaching. Note increase of CFP fluorescence (ex: 405 nm; em: 476–496 nm) after YFP (ex: 514 nm; em: 530–550 nm) photobleaching. FM4-64: ΔF image of synaptic vesicle turnover during maximal stimulation (600 APs @ 10 Hz). Arrowhead: FM$^+$ punctum which is colocalized with YFP/CFP.

(E) Summary of E_{mini} data for GB$_{1a}^{CFP}$ only (n = 18, N = 5), GB$_{1a}^{CFP}$/TNFR$_2^{YFP}$ (n = 11, N = 4), GB$_{1a}^{CFP}$/GB$_2^{YFP}$ (n = 38, N = 7), and Gγ$_2^{N'\text{-}CFP}$/Gβ$_1^{N'\text{-}YFP}$ (n = 13, N = 4), Gγ$_2^{N'\text{-}CFP}$/TNFR$_2^{YFP}$ (n = 9, N = 3). E_{mini} for GB$_{1a}^{CFP}$/GB$_2^{YFP}$ and Gγ$_2^{N'\text{-}CFP}$/Gβ$_1^{N'\text{-}YFP}$ were significantly higher ($p < 0.0001$) than nonspecific GB$_{1a}^{CFP}$/TNFR$_2^{YFP}$ and Gγ$_2^{N'\text{-}CFP}$/TNFR$_2^{YFP}$ interactions. Scale bars: 10 μm (A$_1$), 2 μm (A$_3$, D). Error bars represent SEM. See also Figure S2.

a given axon, contributing to a nonuniform inhibition of vesicle release in hippocampal neurons. Variability in GABA$_B$R activation arises from local differences in basal [GABA]$_o$ in the vicinity of synapses. The presynaptic GABA$_B$R tone is differentially regulated along the dendritic tree and homeostatically controlled by prolong changes in neuronal activity. These data suggest a critical role for GB$_{1a}$/GB$_2$ receptor in local regulation of release probability and its adaptation to changes in ongoing activity.

RESULTS

GABA$_B$R FRET Reveals Variability at Single Excitatory Boutons

Binding of GABA to the GABA$_B$R and subsequent receptor activation is the first step toward producing presynaptic inhibition. To explore the regulation of transmitter release by the presynaptic GB$_{1a}$/GB$_2$ receptors at individual hippocampal synapses, we searched for an optical detector of GABA$_B$R activation by endogenous GABA. We utilized FRET spectroscopy to study conformational changes between fluorescently tagged GB$_{1a}$ (GB$_{1a}^{CFP}$) and GB$_2$ (GB$_2^{YFP}$) receptor subunits (Fowler et al., 2007). FRET provides an accurate measure of possible changes in the relative distance (<100 Å) and/or orientation between the fluorophores. First, we explored interactions between GB$_{1a}^{CFP}$ and GB$_2^{YFP}$ proteins expressed at excitatory boutons in cultured pyramidal hippocampal neurons (Figures 1A and 1B). Presynaptic localization of the tagged GABA$_B$Rs in boutons was confirmed by colocalization of GB$_{1a}^{YFP}$ receptor subunit with CFP-tagged synapsin Ia protein (Syn$_{1a}^{CFP}$; see Figure S1A available online) and with FM4-64 dye (Figure 1D), a marker of presynaptic vesicle turnover. We measured the steady-state FRET efficiency (E) utilizing the acceptor photobleaching method (Figures 1C, 1D, and S1B–S1E), which dequenches the donor (CFP). FRET efficiency was measured under miniature synaptic activity (E_{mini}) in the presence of tetrodotoxin (+TTX), which inhibits spike-dependent neurotransmitter release.

To estimate E_{mini} using a spectroscopic approach, CFP/YFP emission were collected in the range of 400–700 nm under 405 nm excitation wavelength, at single presynaptic boutons expressing GB$_{1a}^{CFP}$ and GB$_2^{YFP}$ proteins. A typical emission spectrum (Figure 1C) and high-magnification confocal images (Figure 1D) at the presynaptic bouton marked by arrowhead in Figures 1A$_2$ and 1A$_3$ show an increase in CFP fluorescence after YFP photobleaching, indicating dequenching of the donor and the presence of FRET. The photobleaching was specific for the selected region of interest and did not produce any detectable damage of presynaptic function (see technical details in Figure S1 and Experimental Procedures). The bouton activity was confirmed by its staining with FM4-64 under maximal electrical stimulation (600 action potentials at a rate of 10 Hz) or high potassium solution (50 mM HiK, 1 min) (Figure 1D). Quantitative analysis of FRET signals between GB$_{1a}^{CFP}$ and GB$_2^{YFP}$ proteins across different boutons along a single axon under miniature synaptic activity revealed a surprising heterogeneity in E_{mini}, with a range of 0.12 to 0.33 and a coefficient of variation (CV = SD/mean) of 34% (Figure S2A). On average, E_{mini} was 0.16 ± 0.01 (CV = 40%) across 38 functional boutons from 7 neurons ($p < 0.0001$; Figure 1E). The observed FRET signals did not depend on the expression level of the acceptor

molecules per bouton (as determined by total YFP fluorescence intensity), on the expression level of the donor molecules per bouton (as determined by CFP fluorescence intensity), and on the donor-to-acceptor ratio (Figures S2B–S2D), excluding these parameters as a potential source of variability. To rule out non specific association due to overexpression of the tagged proteins, we cotransfected GB_{1a}^{CFP} and a nonrelated tumor necrosis factor receptor 2, C terminally tagged with YFP ($TNFR_2^{YFP}$). These two CFP/YFP tagged proteins showed negligible FRET (0.023 ± 0.004, n = 11; Figure 1E). Furthermore, background enhancement of CFP emission, assessed by photobleaching at 514 nm in neurons expressing only GB_{1a}^{CFP}, was <3% (0.027 ± 0.003, n = 18; Figure 1E). Therefore, the higher FRET efficiencies measured with GB_{1a}^{CFP} and GB_2^{YFP} ($p < 0.0001$) are due to specific association of GB_{1a}^{CFP} and GB_2^{YFP} proteins in functional boutons.

To determine whether the variability of FRET was unique for the GB_{1a}/GB_2 heterodimer, we measured the FRET between another known heterodimer, the $G\beta_1\gamma_2$ G protein subunits (Figure 1B). In contrast to the variable FRET between GB_{1a}^{CFP} and GB_2^{YFP} receptor subunits, the FRET between β_1^{YFP} and γ_2^{CFP} proteins across boutons was uniform (CV = 8%) and higher (0.23 ± 0.005, n = 13; Figures 1E and S2E–S2G). Background FRET was negligible between $TNFR_2^{YFP}$ and $G\gamma_2^{N'\text{-}CFP}$ (0.02 ± 0.005, n = 9; Figure 1E). Taken together, these results suggest that the variability in FRET is a specific feature of the GB_{1a}/GB_2 association.

Basal $[GABA]_o$ Regulates Local GB_{1a}/GB_2 Association at Excitatory Boutons

We next investigated the possible source of inter-synapse GB_{1a}/GB_2 FRET variability at excitatory boutons. We hypothesized that variations in local extracellular GABA concentration ($[GABA]_o$) in the vicinity of synapses during miniature synaptic activity might account for the variability. To examine this possibility, we compared FRET efficiency between GB_{1a}^{CFP} and GB_2^{YFP} measured under miniature synaptic activity (+TTX, E_{mini}) and FRET efficiency measured at nonfunctional boutons lacking synaptic vesicle release (E_{rest}). We utilized two different strategies to create inactive boutons (Figure S3): (1) block of SNARE-mediated vesicle release by tetanus toxin (TeTx); (2) investigating immature boutons of young neurons (4–5 DIV). In contrast to the high variability of E_{mini} (CV = 39%), E_{rest} was less variable between GB_{1a}^{CFP} and GB_2^{YFP} proteins in boutons of neurons lacking synaptic vesicle release. The CV decreased to ~14% in both TeTx-treated and immature neurons (Figure 2A). In addition, mean E_{rest} was significantly lower ($p < 0.01$) in either TeTx-treated (0.12 ± 0.03, n = 24) or immature neurons (0.11 ± 0.005, n = 15), compared to E_{mini} under basal conditions (0.16 ± 0.02; n = 20). These results indicate that in the absence of SNARE-mediated neurotransmitter release, GB_{1a}^{CFP}/GB_2^{YFP} FRET signals do not significantly vary across boutons. We propose that miniature vesicle release promotes FRET between GB_{1a}^{CFP} and GB_2^{YFP} proteins by a variable degree according to local GABA levels in the vicinity of boutons. Increase in FRET between GB_{1a}^{CFP} and GB_2^{YFP} proteins could be due to either change in the conformation of pre-existing dimers or to the equilibrium between monomers and dimers. As several studies indicate that heterodimerization of GB_{1a}/GB_2 is required for functional receptor expression (Jones et al., 1998; Kaupmann et al., 1998; White et al., 1998), we favor the interpretation that activity-dependent conformational changes occur in GB_{1a}/GB_2 heterodimers. Altogether, these results confirm that formation of GB_{1a}^{CFP}/GB_2^{YFP} heterodimers does not require synaptic activity and suggest that intrinsic GB_{1a}^{CFP}/GB_2^{YFP} associations do not contribute to the observed inter-synapse FRET variability under miniature synaptic activity.

To explore whether levels of GABA were involved in determining the extent of FRET between GB_{1a}^{CFP} and GB_2^{YFP} at individual boutons, we assessed the effect of different pharmacological manipulations. We first measured E_{mini}s before and after application of the competitive selective $GABA_BR$ antagonist CGP54626 for different population of boutons in the same axon. Interestingly, CGP54626 (1 μM) reduced both the CV (from 41% to 19%) and the mean E_{mini} for GB_{1a}^{CFP} and GB_2^{YFP} (from 0.17 ± 0.016 to 0.12 ± 0.007, n = 12–15, $p < 0.01$; Figure 2B, left graph). Notably, CGP54626 did not affect E_{rest} in the absence of GABA release (n = 14–16, $p > 0.4$; Figure 2B, right graph), suggesting a specific effect of the antagonist on released GABA. To test the effect of antagonist at the same population of boutons (i.e., without photobleaching), we monitored the ratio of YFP to CFP emission (F_{YFP}/F_{CFP}) under CFP excitation before and after CGP54626 application. CGP54626 reversibly reduced F_{YFP}/F_{CFP} ratio and decreased its variability ($p < 0.001$; Figures S4A–S4C), similar to the donor dequenching method.

Because antagonizing basal GABA reduced the FRET between GB_{1a}^{CFP} and GB_2^{YFP}, we hypothesized that maximal receptor activation would increase the FRET efficiency but also reduce the variability. To investigate this possibility, we examined the effect of a saturating dose of baclofen, a competitive selective agonist of $GABA_BR$s. Baclofen (10 μM) increased E_{mini} between GB_{1a}^{CFP} and GB_2^{YFP} subunits to 0.29 ± 0.007 (n = 12, $p < 0.0001$; Figure 2C, left graph) with a concomitant ~5-fold reduction of CV to 8%. Notably, baclofen induced strong FRET in immature neurons (n = 9, $p < 0.0001$; Figure 2C, right graph). Baclofen also increased the F_{YFP}/F_{CFP} ratio and reduced signal variability at the same population of boutons (n = 9, $p < 0.001$; Figure S4D). The observed baclofen-induced increase in FRET reversed upon washout (Figures S4D and S4E). The effect of baclofen on GB_{1a}^{CFP}/GB_2^{YFP} FRET was specific since it did not induce FRET between GB_{1a}^{CFP} and $TNFR_2^{YFP}$ proteins (Figure S4F). These results complement recent FRET study on agonist-induced rearrangements between GB_{1a} and GB_2 subunits tagged at intracellular loops (Matsushita et al., 2010).

Next, we examined whether GABA uptake affects GB_{1a}/GB_2 interactions through regulation of $[GABA]_o$ under miniature synaptic activity. The specific GABA transporter inhibitor SKF-89976A (25 μM) was used to raise $[GABA]_o$. Blocking GABA uptake induced ~2-fold increase in the mean level of E_{mini} from 0.13 ± 0.01 to 0.27 ± 0.02, while decrease in CV from 43% to 24% (n = 14–15, $p < 0.0001$; Figure 2D). Thus, similar to baclofen, elevating $[GABA]_o$ drives $GABA_BR$s to an activated state (high FRET). Furthermore, these results suggest that GABA transporter activity contributes to the heterogeneity of $[GABA]_o$ and GB_{1a}/GB_2 FRET.

Finally, we probed the pattern of GB_{1a}^{CFP}/GB_2^{YFP} interactions under GABA release evoked by action potentials (Figure 2E).

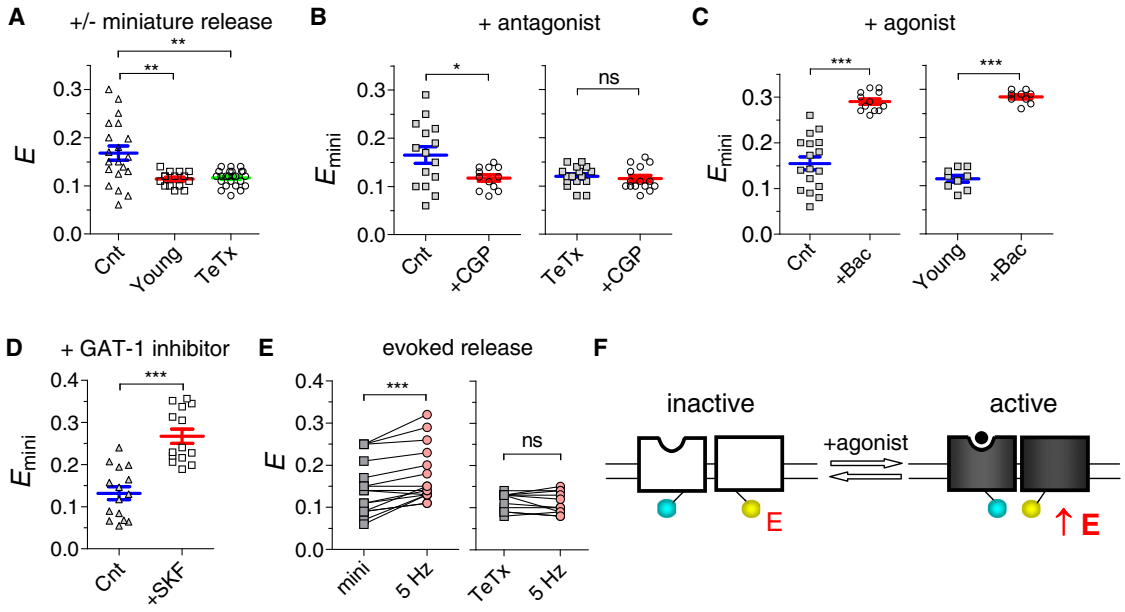

Figure 2. Analysis of Intersynapse Heterogeneity of GB_{1a}/GB_2 Associations at Excitatory Boutons

(A) FRET efficiency between GB_{1a}^{CFP} and GB_2^{YFP} in functional boutons under miniature activity (+TTX, control group, 0.16 ± 0.02, CV = 39%, n = 20, N = 5) and nonfunctional boutons: TeTx-pretreated (0.12 ± 0.03, CV = 14%, n = 24, N = 6) and immature (4–5 DIV, 0.11 ± 0.005, CV = 14%, n = 15, N = 4) neurons. Mean *E* is lower and less variable in nonfunctional boutons.

(B) CGP54626 (1 μM) reduced mean E_{mini} to 0.12 ± 0.007 and its variability to CV = 19% in control (left, n = 12–15, N = 4), but not in TeTx-treated neurons (right, n = 14–16, N = 4).

(C) Baclofen (10 μM) increased mean E_{mini} and reduced its variability in control (left, 0.29 ± 0.007, CV = 8%, n = 12–17, N = 4, $p < 0.0001$) and in immature (right, 0.28 ± 0.004, CV = 5%, n = 9, N = 3 $p < 0.0001$) neurons.

(D) SKF-89976A (25 μM) increased mean E_{mini} (0.27 ± 0.02, n = 14–15, N = 4, $p < 0.0001$) and decreased CV from 43% to 24%.

(E) Left: Comparison of *E* monitored under miniature activity and during 5 Hz stimulation (both conditions in the presence of kynurenic acid) over the same population of synapses in control neurons (n = 16, N = 4). Stimulation increased mean *E* ($p < 0.001$) but did not affect CV (44% and 38% for mini and 5 Hz, respectively). Right: In TeTx-treated neurons, 5 Hz did not affect *E* (n = 11, N = 3, $p > 0.4$).

(F) Schematic illustration of increase in FRET within the GB_{1a}^{CFP}/GB_2^{YFP} heterodimer by endogenous $[GABA]_o$.

Error bars represent SEM. See also Figure S4.

In these experiments, recurrent network activity was blocked by a nonselective antagonist of ionotropic glutamate receptors (kynurenic acid). Activity-induced FRET changes were reversible (Figure S4G), enabling FRET monitoring under miniature (no stimulation) versus evoked (by 5 Hz field stimulation) release at the same population of boutons. Interestingly, evoked release produced ~20% increase in the mean *E* and preserved the variability (CV = 38%, n = 16; Figure 2E, left graph). Importantly, 5 Hz stimulation did not change FRET in nonreleasing TeTx-treated neurons (n = 11, $p > 0.4$; Figure 2E, right graph), indicating the requirement for synaptic release of GABA.

Taken together, these data suggest that (1) GB_{1a}^{CFP}/GB_2^{YFP} form stable dimers in the absence of synaptic activity and change their conformation in response to agonist (Figure 2F); (2) GB_{1a}/GB_2 FRET variability decreases in the absence of synaptic activity, indicating homogeneity of GB_{1a}/GB_2 assembly; (3) $[GABA]_o$ near synaptic contacts induces partial GABA$_B$R activation per excitatory bouton and underlies variability of GB_{1a}/GB_2 associations under basal synaptic activity. Therefore, C terminally tagged GB_{1a}/GB_2 receptor subunits provide highly sensitive detectors for $[GABA]_o$ in the vicinity of excitatory synapses and for GABA$_B$R activation.

Although presynaptic GB_{1a}/GB_2 receptors are predominantly localized at excitatory boutons as heteroreceptors, a fraction of GABAergic terminals expresses GB_{1a}/GB_2 autoreceptors (Vigot et al., 2006). We detected only 7% (3/41) of inhibitory cells, which expressed (GB_{1a}^{CFP} + GFP) proteins from whole population of the transfected cells, comparing to 30% (15/49) of inhibitory cells that expressed GFP alone. Inhibitory cells were identified by the lack of spines and by immunostaining with GAD-65 antibody after FRET measurements. To compare the properties of auto- versus heteroreceptors, we analyzed FRET efficiencies at a fraction of inhibitory boutons expressing GB_{1a}^{CFP}/GB_2^{YFP} autoreceptors (Figure 3A). Under miniature synaptic activity, FRET efficiencies at inhibitory boutons were higher (0.21 ± 0.01, n = 12; Figure 3B, control) and less variable (CV = 16.6%) than at excitatory ones (Figure 2). In the absence of synaptic activity, FRET efficiencies within the autoreceptors reduced to ~10% (0.11 ± 0.005 and 0.10 ± 0.006, n = 9–13, $p < 0.001$, for immature and TeTx-treated neurons, respectively; Figure 3B), similarly to the E_{rest} levels measured within the heteroreceptors. Application of CGP54626 antagonist also resulted in a reduction of E_{mini} to the E_{rest} level (0.10 ± 0.008, n = 9–11, $p < 0.0001$; Figure 3C), suggesting higher basal $[GABA]_o$ in the

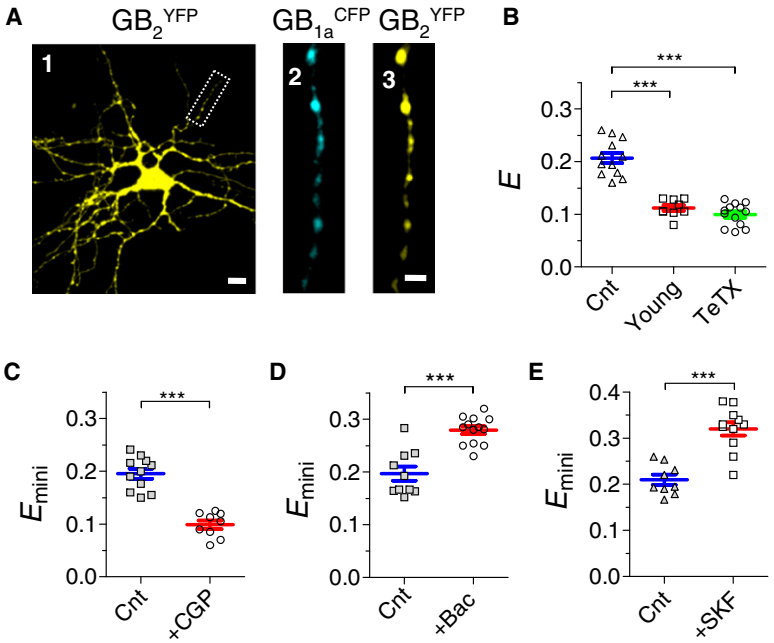

Figure 3. Analysis of GB$_{1a}$/GB$_2$ Associations at Inhibitory Boutons

(A) Representative confocal images of an inhibitory neuron in hippocampal culture that was cotransfected with GB$_2^{YFP}$ and GB$_{1a}^{CFP}$. White box in (A$_1$) corresponds to the blow-ups in (A$_2$) and (A$_3$). Scale bars: 10 μm (A$_1$), 2 μm (A$_3$).

(B) FRET efficiency between GB$_{1a}^{CFP}$ and GB$_2^{YFP}$ in functional boutons under miniature activity (+TTX, control group, 0.21 ± 0.01, CV = 16%, n = 12, N = 4) and nonfunctional boutons: TeTx-pretreated (0.10 ± 0.006, CV = 20%, n = 13, N = 3) and immature (0.11 ± 0.005, CV = 15%, n = 9, N = 3) neurons.

(C) The GABA$_B$R competitive antagonist CGP54626 (1 μM) reduced mean E_{mini} to 0.10 ± 0.008 (CV = 23%, n = 9–11, N = 2).

(D) The GABA$_B$R competitive agonist baclofen (10 μM) increased mean E_{mini} to 0.28 ± 0.07, (CV = 9%, n = 10–13, N = 3, $p < 0.01$).

(E) GABA uptake inhibitor SKF-89976A (25 μM) increased mean E_{mini} to 0.32 ± 0.01 (CV = 15%, n = 9–11, N = 2, $p < 0.0001$).

Error bars represent SEM.

vicinity of GB$_{1a}^{CFP}$/GB$_2^{YFP}$ autoreceptors. Conversely, E_{mini}s were increased by baclofen (0.28 ± 0.007, n = 10–13, $p < 0.01$; Figure 3D) and GABA transporter blocker SKF-89976A (0.32 ± 0.014, n = 9–11, $p < 0.0001$; Figure 3E).

In summary, FRET measurements at GABAergic boutons suggest that (1) in the absence of synaptic activity, assembly of GB$_{1a}$/GB$_2$ autoreceptors is similar to those of heteroreceptors; (2) activation of GB$_{1a}$/GB$_2$ autoreceptors is stronger and less variable due to higher local [GABA]$_o$. Therefore, GB$_{1a}$/GB$_2$ autoreceptors, although expressed only in ~23% of GABAergic boutons, may induce autoinhibition of quantal GABA release, and, therefore, contribute to intersynapse variability of basal [GABA]$_o$.

Agonist-Induced Uniform GABA$_B$R Activation

We then examined the potency of baclofen to induce conformational changes in the GB$_{1a}$/GB$_2$ heterodimer. First, we used HEK293 cells as a heterologous expression system to examine possible agonist-induced FRET changes between the tagged GB$_{1a}$ and GB$_2$ receptor subunits (Figure S5A). Utilizing donor-dequenching method, we measured FRET efficiency of 0.095 ± 0.004 under resting conditions (Figures S5B and S5C), similarly to previous results (Fowler et al., 2007). FRET did not depend on the expression levels of acceptor, donor, and donor/acceptor ratio (Figures S5D–S5F). To test FRET signals before and after baclofen application, we utilized nondestructive sensitized emission methodology. Baclofen induced dose-dependent reversible increase in FRET (n = 10, $p < 0.01$; Figure S5G), accompanied by an increase in G protein-gated inwardly rectifying potassium currents (n = 10; Figure S5H) as a readout of receptor activation. These data suggest that agonist-induced increase in FRET between the C terminally tagged GB$_{1a}$/GB$_2$ receptor subunits reflects receptor activation.

Then, we measured the potency of baclofen to induce conformational changes in the GB$_{1a}^{CFP}$/GB$_2^{YFP}$ receptor expressed in presynaptic boutons and compared to changes in presynaptic Ca^{2+} transients and in basal vesicle release. Baclofen dose-response curve for FRET efficiency between GB$_{1a}^{CFP}$ and GB$_2^{YFP}$ revealed an ED$_{50}$ of 0.83 ± 0.006 μM (n = 8–10; Figure 4A), which is comparable to the affinity for native GB$_{1a}$/GB$_2$ receptors (~0.6 μM; Malitschek et al., 1998). Next, we constructed a dose-response curve for baclofen inhibition on presynaptic Ca^{2+} transients. Functional boutons were identified by FM4-64 marker (Figure 4B). Presynaptic Ca^{2+} transients evoked by low-frequency stimulation were measured by high-affinity fluorescent calcium indicator Oregon Green 488 BAPTA-1 AM. Baclofen had no effect on resting Ca^{2+}-dependent fluorescence, while decreased the size of action-potential dependent fluorescence transients ($\Delta F/F$; Figure 4B). Baclofen induced concentration-dependent inhibition of presynaptic Ca^{2+} transients with maximal inhibition level of ~20% and ED$_{50}$ of 0.46 ± 0.01 μM (n = 10–15; Figure 4A), similarly to its effect in hippocampal slices (Wu and Saggau, 1995). Finally, we estimated the potency of baclofen on inhibition of synaptic vesicle turnover. Activity-dependent FM1-43 dye has been used to estimate changes in basal synaptic vesicle turnover at hippocampal synapses (Abramov et al., 2009). We quantified the total amount of releasable fluorescence (ΔF) at each bouton following stimulation by 30 action potentials at a rate of 0.2 Hz in the presence of 10 μM FM1-43 and subsequent destaining (Figures S6A and S6B). Analysis of baclofen (1 μM) effect revealed an average decrease of ΔF across synapses (Figures 4C and 4D). The effect of baclofen was uniform across boutons, no correlation was found between presynaptic changes and initial ΔF values (Spearman r = –0.1, $p > 0.2$; Figure 4E). Given that baclofen inhibits FM destaining rate (Figure S7) without affecting synaptic

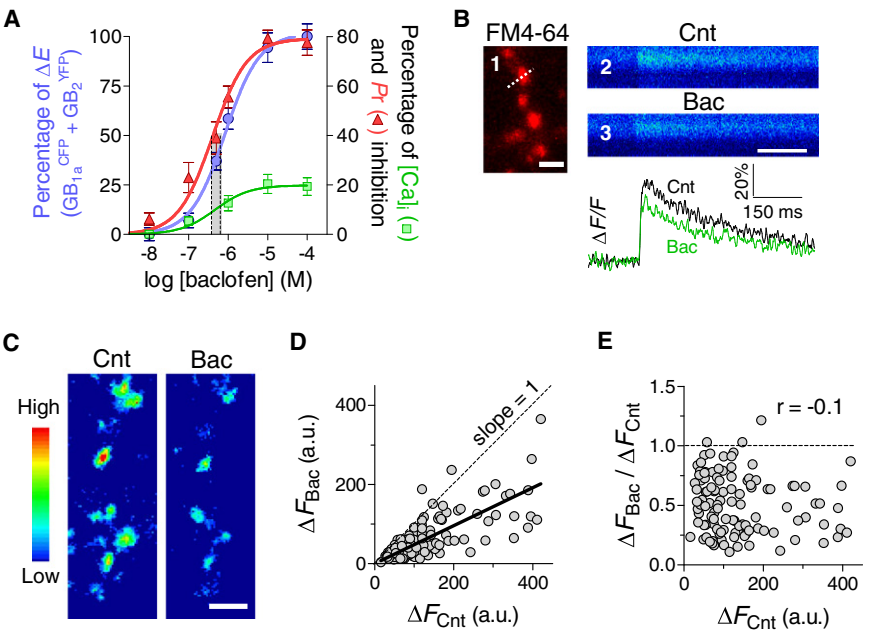

Figure 4. Baclofen Displays Similar Potency for GB$_{1a}$/GB$_2$ Conformational Changes and Presynaptic Inhibition of [Ca^{2+}]$_i$ and Basal Vesicle Release

(A) Dose-response curves of baclofen on *E* between GB$_{1a}$^{CFP}and GB$_2$^{YFP} proteins (n = 8–10, ED$_{50}$ = 0.83 ± 0.006 μM), on presynaptic Ca^{2+} transients (n = 10–15, ED$_{50}$ = 0.46 ± 0.01 μM), and on presynaptic activity measured by FM1-43 dye (n = 4–7, ED$_{50}$ = 0.40 ± 0.06 μM). *E* at 100 μM baclofen was set as 100%.

(B) Activation of GABA$_B$Rs with baclofen reduced spike-dependent presynaptic Ca^{2+} entry. Functional presynaptic boutons were detected by FM4-64 dye staining (B$_1$, dotted line shows position of line scan). Ca^{2+} transients were evoked by 0.2 Hz stimulation during 500 Hz line scan of boutons before and after baclofen application (B$_2$ and B$_3$). Ca^{2+} transients were quantified as Δ*F*/*F* before (black) and after (green) baclofen application (average of 10 traces). Scale bar: 150 ms (B$_3$), 2 μm (B$_1$).

(C) Representative Δ*F*$_{FM1-43}$ images before and 10 min after 1 μM baclofen application. Stimulation during FM1-43 staining: 30 action potentials at 0.2 Hz (see Figures S6A and 6B for details). Scale bar: 2 μm. Fluorescence intensities (arbitrary units) are coded using a pseudocolor transformation.

(D) Single-synapse analysis of baclofen effect across 118 boutons (slope of linear fit is 0.47 ± 0.02). Dotted line designates no change (slope = 1).

(E) Baclofen-induced inhibition did not correlate to initial presynaptic strength (Spearman r = –0.1, p > 0.2, the same data as in D).

Error bars represent SEM. See also Figure S6.

vesicle endocytosis (Isaacson and Hille, 1997), the observed baclofen-induced reduction in Δ*F* signals primarily reflects inhibition of vesicle exocytosis. Applying this method for construction of a full dose-response curve, we estimated an ED$_{50}$ of 0.40 ± 0.06 μM for baclofen-induced presynaptic inhibition in our experimental system (Figure 4A). The similarity in potency of baclofen to increase GB$_{1a}$/GB$_2$ FRET and to inhibit both presynaptic Ca^{2+} transients and vesicle release indicates a tight coupling between the GB$_{1a}$/GB$_2$ conformational dynamics and functional activation of presynaptic GABA$_B$ receptors.

Variability of Basal GABA$_B$R-Mediated Presynaptic Inhibition

To assess the role of GABA$_B$Rs in presynaptic inhibition induced by basal GABA release, we quantified synaptic vesicle recycling at hippocampal synapses before and after application of the GABA$_B$R antagonist. First, we tested CGP54626 effects on basal vesicle release evoked by low frequency (0.2 Hz) stimulation. Under these conditions, CGP54626 nonuniformly increased fluorescence intensity of FM1-43 signals at individual boutons (Figure 5A). Analysis of the CGP54626 effect across 236 boutons revealed an average increase of Δ*F* across synapses (Figure 5B). However, in contrast to uniform effect induced by agonist (Figure 4E), antagonist predominantly affected boutons exhibiting low initial Δ*F* values (Figure 5C; Spearman r = −0.9, p < 0.0001). At the level of synaptic population, CGP54626 increased the total presynaptic strength, defined as *S* = Δ*F* × *D*, whereas *D* is the density of FM$^+$ boutons per image area (1.66 ± 0.92, N = 6, p < 0.0001; Figure 5D). In addition to enhancement of evoked basal presynaptic strength (0.2 and 1 Hz, Figure 5D), CGP54626 increased miniature presynaptic strength by similar extent (1.56 ± 0.16, N = 6, p > 0.5; Figure 5D) in a nonuniform manner (Spearman r = –0.6, p < 0.0001). Taken together, these results suggest that under both miniature and evoked basal synaptic activity GABA$_B$Rs are activated by GABA, leading to a synapse-specific presynaptic inhibition.

GB$_{1a}$/GB$_2$ Associations Correlate to *Pr* at Single Synapses

To assess the influence of GB$_{1a}$/GB$_2$ conformational state on tonic inhibition of synaptic vesicle release, we simultaneously monitored the effect of GABA$_B$R antagonist on GB$_{1a}$^{CFP}/GB$_2$^{YFP} FRET ratio and on basal vesicle recycling at individual synapses of pyramidal neurons. Neuronal cultures expressing GB$_{1a}$^{CFP} and GB$_2$^{YFP} fusion proteins were subjected to FM4-64 staining under evoked (by 0.2 Hz stimulation) or miniature (+TTX) synaptic activity. Ectopic expression of GB$_{1a}$^{CFP}/GB$_2$^{YFP} fusion proteins did not affect the level of baclofen-induced presynaptic inhibition (Figures S6C and S6D). Figure 5E demonstrates differential effect of CGP54626 antagonist at two boutons under 0.2 Hz stimulation. At the bouton #1, CGP54626 induced a ~25% decrease in F_{YFP}/F_{CFP} (due to increase in F_{CFP} with concomitant reduction in F_{YFP}) and an ~96% increase in ΔF_{FM4-64}. In contrast, CGP54626 did not significantly alter either F_{YFP}/F_{CFP} or ΔF_{FM4-64} at the bouton #2. The pooled data (Figure 5F) demonstrate a correlation between the degree of antagonist-induced decrease in F_{YFP}/F_{CFP} ratio within the GB$_{1a}$^{CFP} and GB$_2$^{YFP} pair and increase in basal synaptic vesicle recycling under evoked (n = 13, Spearman

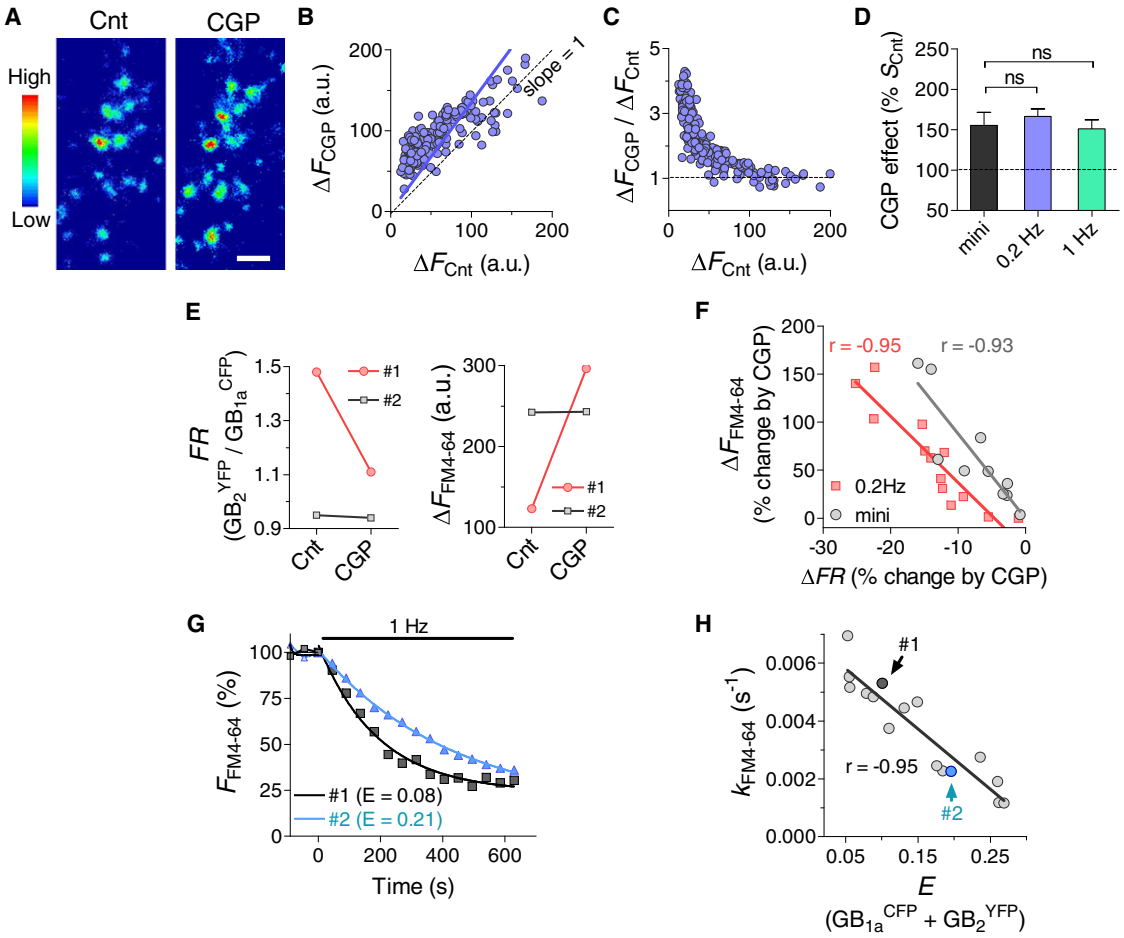

Figure 5. Basal GABA$_B$R Activation Negatively Correlates to Release Probability at the Single-Bouton Level

(A) Representative $\Delta F_{FM1\text{-}43}$ images before and 10 min after application of 1 μM CGP54626. Stimulation during FM1-43 staining: 30 action potentials at 0.2 Hz. Destaining: 1000 action potentials at 2 Hz. Fluorescence intensities (arbitrary units) are coded using a pseudocolor transformation. Scale bar: 2 μm.

(B and C) CGP54626 effect at the level of single synapses. Slope of linear fit is 1.35 ± 0.03 (n = 236, B). Dotted line denotes no change (slope = 1). CGP54626-induced augmentation is inversely correlated to initial presynaptic strength (Spearman r = - 0.9, p < 0.0001, C).

(D) Comparison of the GABA$_B$R-mediated presynaptic inhibition under miniature versus evoked (stimulation frequency of 0.2 and 1 Hz) basal release. CGP54626 displayed similar degree of presynaptic enhancement on miniature and evoked basal presynaptic strength (6–9 experiments per group, p > 0.5).

(E) Representative data demonstrating effects of 1 μM CGP54626 on $\Delta F_{FM4\text{-}64}$ and F_{YFP}/F_{CFP} ratio during 0.2 Hz stimulation at two boutons expressing GB_{1a}^{CFP} and GB_2^{YFP} proteins. CGP54626 significantly changed both F_{YFP}/F_{CFP} and $\Delta F_{FM4\text{-}64}$ in the bouton #1, while produced only minor changes on F_{YFP}/F_{CFP} and $\Delta F_{FM4\text{-}64}$ in the bouton #2.

(F) Pooled data show negative correlation between the effect of CGP54626 on F_{YFP}/F_{CFP} ($\Delta FR = FR_{CGP}/FR_{Cnt} - 1$) × 100%) and on evoked (13 boutons, Spearman r = –0.95, p < 0.0001, red symbols) or miniature (10 boutons, Spearman r = –0.93, p < 0.0001, gray symbols) synaptic vesicle turnover ($\Delta F = (\Delta F_{CGP}/\Delta F_{Cnt} - 1) \times 100\%$).

(G) Representative data demonstrating correlation between GB_{1a}^{CFP}/GB_2^{YFP} FRET efficiency (E) and FM4-64 destining rate constant during 1 Hz stimulation (k) in two boutons expressing GB_{1a}^{CFP} and GB_2^{YFP}.

(H) Pooled data across 16 boutons reveal negative correlation between E within the GB_{1a}^{CFP}/GB_2^{YFP} heterodimer and FM4-64 decay rate constant (Spearman r = –0.95, p < 0.0001).

Error bars represent SEM. See also Figure S7.

r = –0.95, p < 0.0001) or miniature (n = 10, Spearman r = –0.93, p < 0.0001) activity at individual boutons. These data indicate that GB_{1a}/GB_2 conformation may predict the level of tonic inhibition at the single-bouton level.

The above relationship suggests that basal vesicle release might be fine-tuned through dynamic regulation of the GB_{1a}/GB_2 receptor conformation. To directly examine the relationship between vesicle exocytosis per se and GB_{1a}/GB_2 associations, we monitored FM destaining kinetics (Figure S7A), a reliable indicator of release probability, together with FRET efficiency measurements between GB_{1a}^{CFP} and GB_2^{YFP} proteins at individual boutons. For this purpose, the total pool of recycling vesicles has been stained by 600 action potentials at a rate of 10 Hz and colocalized FM4-64/CFP/YFP puncta were subjected to FRET analysis. The FM4-64 destaining rate and FRET efficiency between GB_{1a}^{CFP} and GB_2^{YFP} subunits

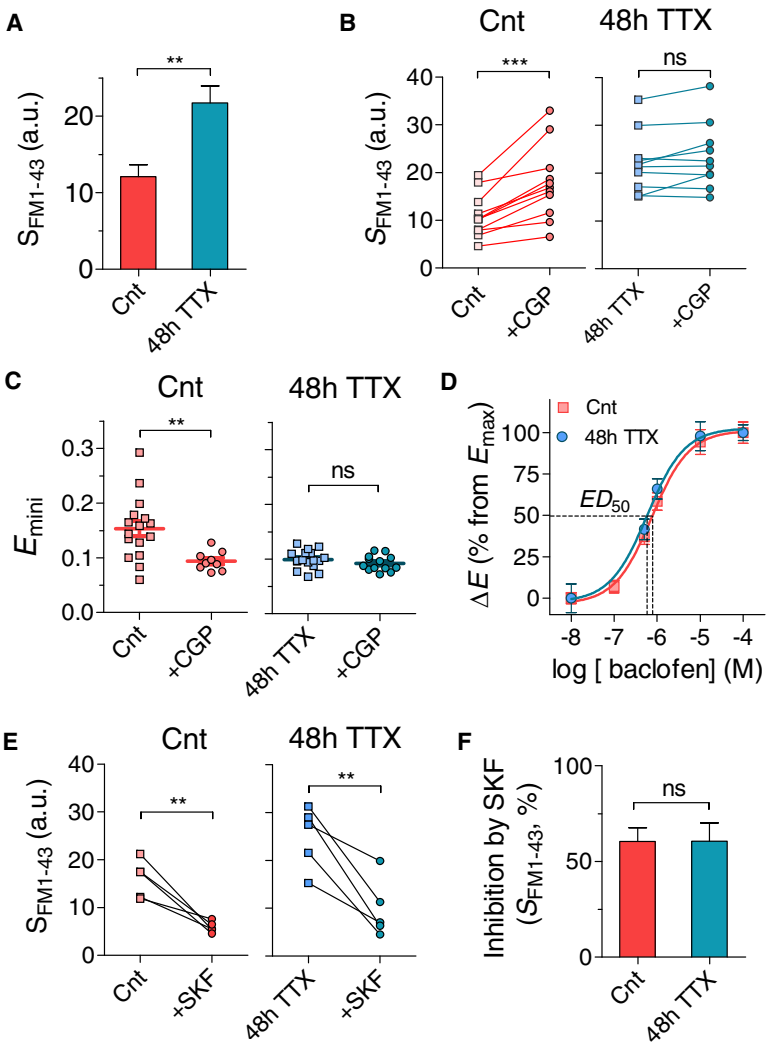

Figure 6. Reduction in the Presynaptic GABA$_B$R Tone by Prolong Activity Blockade

(A) Activity blockade by TTX (48 h) increased miniature presynaptic strength across synaptic populations (S_{FM1-43}, N = 10–13, p < 0.01).

(B) Activity blockade reduced the effectiveness of CGP54626 to increase miniature presynaptic strength (p < 0.0001). CGP54626 (1 μM) increased S_{FM1-43} by (1.6 ± 0.09)-fold in control (left, N = 11, p < 0.0001), but only by (1.06 ± 0.04)-fold in TTX-treated neurons (right, N = 10, p > 0.05).

(C) Activity blockade reduced the effectiveness of CGP54626 to decrease E_{mini} (p < 0.0001). CGP54626 (1 μM) decreased E_{mini} from 0.15 ± 0.01 to 0.09 ± 0.006 (left, n = 9–16, N = 4, p < 0.01) with concurrent reduction in CV from 38% to 19% in control cultures. In TTX-treated cultures, CGP54626 changed neither the mean level nor the variability of E_{mini} (right, n = 13–17, N = 4, p > 0.2).

(D) Dose-response curve of baclofen on E_{mini} between GB_{1a}^{CFP} and GB_2^{YFP} proteins in control (n = 7–10, N = 4, ED_{50} = 0.7 ± 0.005 μM) versus TTX-treated (n = 7–13, N = 4–5, ED_{50} = 0.6 ± 0.004 μM) cultures.

(E) Reduction of basal presynaptic strength by GABA uptake inhibitor SKF-89976A (25 μM) in control (N = 5, p < 0.01) versus TTX-treated (N = 5, p < 0.01) cultures.

(F) Activity blockade did not alter the effectiveness of SKF-89976A to decrease presynaptic strength in control versus TTX-treated cultures (N = 5, p > 0.9)

Error bars represent SEM. See also Figure S8.

have been measured during 1 Hz stimulation. The FM destaining rate constant ($k = 1/\tau_{decay}$, whereas τ_{decay} is an exponential time course) is proportional to probability of vesicle release. The destaining rate constant was plotted against GB_{1a}^{CFP}/GB_2^{YFP} FRET efficiency per bouton. Figure 5G demonstrates two boutons with different FRET levels: the bouton #1 displays smaller increase in F_{CFP} following YFP photobleaching than the bouton #2 (left graph), resulting in lower FRET (0.085 versus 0.21). Notably, the bouton #2 is characterized by higher FRET and slower detaining rate (k was 0.0024 versus 0.0052 s^{-1}, for #2 and #1, respectively; Figure 5G). The pooled data from 16 boutons demonstrate an inverse correlation between the initial GB_{1a}^{CFP}/GB_2^{YFP} FRET efficiency and the rate of FM destaining per bouton (Spearman r = –0.95, p < 0.0001; Figure 5H), where greater FRET correlates with slower release of synaptic vesicles. These results suggest variable levels of basal $[GABA]_o$ impact glutamate release probability through tuning of GABA$_B$R signaling, which is detected by GB_{1a}/GB_2 conformational state.

Inactivity Reduces Presynaptic GABA$_B$R Tone

Release probability of individual synapses can be modified by brief periods of temporospatially correlated activity and by prolonged changes in ongoing activity. In hippocampal cultures, strong evidence exists on augmentation of release probabilities (Branco et al., 2008; Murthy et al., 2001; Thiagarajan et al., 2005) with concomitant reduction in release heterogeneity (Branco et al., 2008) as a homeostatic response to prolong synaptic disuse. However, molecular mechanisms that underlie presynaptic disuse hypersensitivity remain largely unknown. If basal activation of GABA$_B$Rs regulates vesicle release probability at a rapid timescale, then changes in the GABA$_B$R tone at a slow timescale might probably underlie homeostatic presynaptic plasticity. To examine this hypothesis, we estimated the GABA$_B$R tone following pharmacological neuronal silencing by TTX for 48 hr. Effects of the GABA$_B$R antagonist were quantified on miniature presynaptic strength measured by FM1-43 and on GB_{1a}/GB_2 activation detected by FRET. As expected, inactivity induced an increase in miniature presynaptic strength across population of synapses (N = 10–13, p < 0.01; Figure 6A). Notably, CGP54626 lost its effectiveness on miniature presynaptic activity in TTX-treated cultures (N = 10, p > 0.05; Figure 6B; right graph), comparing to control ones (N = 11, p < 0.0001; Figure 6B; left graph). Moreover, inactivity induced reduction in GB_{1a}^{CFP}/GB_2^{YFP} FRET efficiency: E_{mini} decreased from 0.15 to 0.10 and its variability from 38 to 17% (n = 16–17, p < 0.001; Figure 6C). Consequently, CGP54626 did not affect GB_{1a}^{CFP}/GB_2^{YFP} FRET

efficiency in TTX-treated cultures (n = 13–17, p > 0.2; Figure 6C, right graph), while efficiently reduced E_{mini} in control cultures (n = 9–16, p < 0.05; Figure 6C, left graph). Two days of TTX treatment did not induce significant changes in the expression levels of GB_{1a}^{CFP}, GB_2^{YFP} or their ratio (Figure S8). Furthermore, the potency of baclofen to increase GB_{1a}^{CFP}/GB_2^{YFP} FRET efficiency was not altered by TTX pretreatment (n = 8–13; Figure 6D), suggesting no changes in responsiveness of the GB_{1a}/GB_2 receptor to agonist. These results suggest decrease in the ambient $[GABA]_o$ as the major determinant of inactivity-induced reduction in the $GABA_BR$ tone. To test if acceleration of GABA clearance might be involved in reduction of basal GABA levels, we tested if the effectiveness of GABA transporter blocker on inhibition of presynaptic strength was increased in TTX-treated cultures. SKF-89976A equally inhibited presynaptic strength by ~60% in control and TTX-treated cultures (N = 5, p < 0.01; Figures 6E and 6F). Therefore, we concluded that inactivity-induced lost of the $GABA_BR$ tone was highly-likely due to reduction in the amount of GABA release (see Discussion).

Presynaptic $GABA_BR$ Tone Is Dendrite Specific

Although release probabilities exhibit high heterogeneity along an axon and within a whole population of hippocampal synapses, this variability is significantly reduced across individual dendritic branches (Branco et al., 2008; Murthy et al., 1997). Notably, release probabilities negatively correlate to the number of synapses on the branch (Branco et al., 2008), suggesting that presynaptic mechanisms might be involved in down-scaling of quantal synaptic weight at heavily innervated dendrites along dendritic tree (Liu and Tsien, 1995). Therefore, we asked whether basal activation of presynaptic $GABA_BRs$ might be regulated at the level of individual dendritic branches. Thus, we compared the effect of $GABA_BR$ antagonist at thick proximal dendrites versus its effect at thin distal dendritic compartments of pyramidal hippocampal neurons. First, we estimated evoked basal vesicle exocytosis by analyzing the FM1-43 destaining rates separately at proximal dendrites with high synapse density (Figure 7A) versus distal dendrites with low synapse density of FM^+ puncta (Figure 7B). CGP54626 induced 2-fold increase in destaining rates of 67 boutons at highly innervated proximal dendrites (destaining rate constant, $k = 1/\tau_{decay}$, was $(1.7 \pm 0.06) \times 10^{-3}$ and $(3.7 \pm 0.13) \times 10^{-3}$ s^{-1}, before and after antagonist application, respectively; Figure 7C). In contrast, CGP54626 did not produce significant change in destaining rates of 71 boutons at distal dendrites (k was $(2.4 \pm 0.06) \times 10^{-3}$ and $(2.6 \pm 0.09) \times 10^{-3}$ s^{-1}, before and after antagonist application, respectively; Figure 7D). Notably, FM^+ boutons at distal dendrites were characterized by higher destaining rates than at proximal one (p < 0.001; Figure 7E, white bars), suggesting higher *Pr*. Both, *Pr* dynamic range from inhibited to noninhibited state (p < 0.0001; Figure 7E, white versus black bars), and intrinsic *Pr* in the absence of $GABA_BR$-mediated inhibition (p < 0.0001; Figure 7E, difference between black bars) were higher at proximal thick dendrites.

To compare the extent of tonic activation of $GABA_BRs$ along dendritic tree under miniature synaptic activity, we measured CGP54626 effects on both presynaptic strength and GB_{1a}^{CFP}/GB_2^{YFP} FRET ratio at boutons contacting proximal versus distal dendrites in the presence of TTX. At proximal branches, CGP54626 increased $\Delta F_{FM1\text{-}43}$ (n = 20, p < 0.0001; Figure 7F, left), while decreasing FRET ratio (n = 8, p < 0.05; Figure 7G, left). However, at distal branches CGP54626 was effective neither at the level of vesicle recycling (n = 20, p > 0.5, Figure 7F, right) nor protein-protein interactions (n = 6, p > 0.6; Figure 7G, right). Moreover, basal FRET ratio was higher at proximal synapses (n = 6 – 8, p < 0.01; Figure 7H), suggesting higher degree of tonic receptor activation. Therefore, the presynaptic $GABA_BR$ tone is differentially regulated along dendritic tree, predominantly impacting proximal synapses.

Next, we examined whether diffusion distance between excitatory and inhibitory synapses is different at proximal thick versus distal thin dendritic branches. As FM dye staining cannot distinguish excitatory from inhibitory synapses, we used both excitatory and inhibitory synapse-specific marker proteins to distinguish between these two types of synapses (Figure S9A). Excitatory synapses were labeled with the vesicular glutamate transporter VGLUT1 antibody, whereas inhibitory synapses were labeled with GABA synthetic enzyme GAD65 antibody. We found that the total number of synapses along a fixed length of dendrite positively correlated to the diameter of the dendritic branch, with higher synapse number at thick proximal dendrites (Spearman r = 0.75, p < 0.0001; Figure S9B), as has been reported in earlier study (Liu, 2004). Interestingly, the ratio of inhibitory to excitatory synapses (N_I/N_E) was positively correlated to dendritic diameter, reaching constant ~0.8 ratio at dendrites with diameter >4 μm (Figure S9C). Altogether, these results suggest that diffusion distance for GABA between inhibitory and excitatory synapses is shorter at thick proximal dendrites.

Finally, we explored location dependency of basal $GABA_BR$-mediated presynaptic inhibition in a more intact preparation, namely in acute hippocampal slices. We compared the presynaptic $GABA_BR$ activation at the most proximal dendrites of CA1 pyramidal neurons in stratum radiatum versus the most distal apical dendrites in stratum lacunosum-moleculare (Figure 8A). Electron microscopy study suggests higher N_I/N_E ratio at proximal dendrites of pyramidal CA1 hippocampal neurons in rat brain (Megías et al., 2001). Because the very thin apical dendrites prevent direct intracellular recordings, we relied on electrophysiological measurements of extracellular field EPSPs (fEPSPs). Given that basal activation of receptors depends on the extracellular levels of transmitters, special care was taken to maintain physiological inhibition-excitation balance and, consequently, neuronal network activity in slices. All recordings were performed under the following conditions: (1) in intact slices without surgical isolation of CA3 region; (2) without blocking of $GABA_A$ receptors; (3) under physiological concentration of $[Ca^{2+}]_o$ and $[Mg^{2+}]_o$ (1.2 mM for both ions) for storage and recording extracellular solutions in order to maintain *Pr*.

First, we assessed the strength of basal synaptic transmission in proximal CA3-CA1 synapses pathway by measuring fEPSPs evoked by low frequency stimulation (0.1 Hz). To test whether presynaptic $GABA_BRs$ are activated under these conditions, we tested the effect of CGP54626 antagonist on the slope of input (amplitude of fiber volley)/output (slope of fEPSP) curve. CGP54626 increased the slope of input/output curve by 40% (from 0.6 ± 0.06 to 1.0 ± 0.05, n = 5, p < 0.01; Figure 8B).

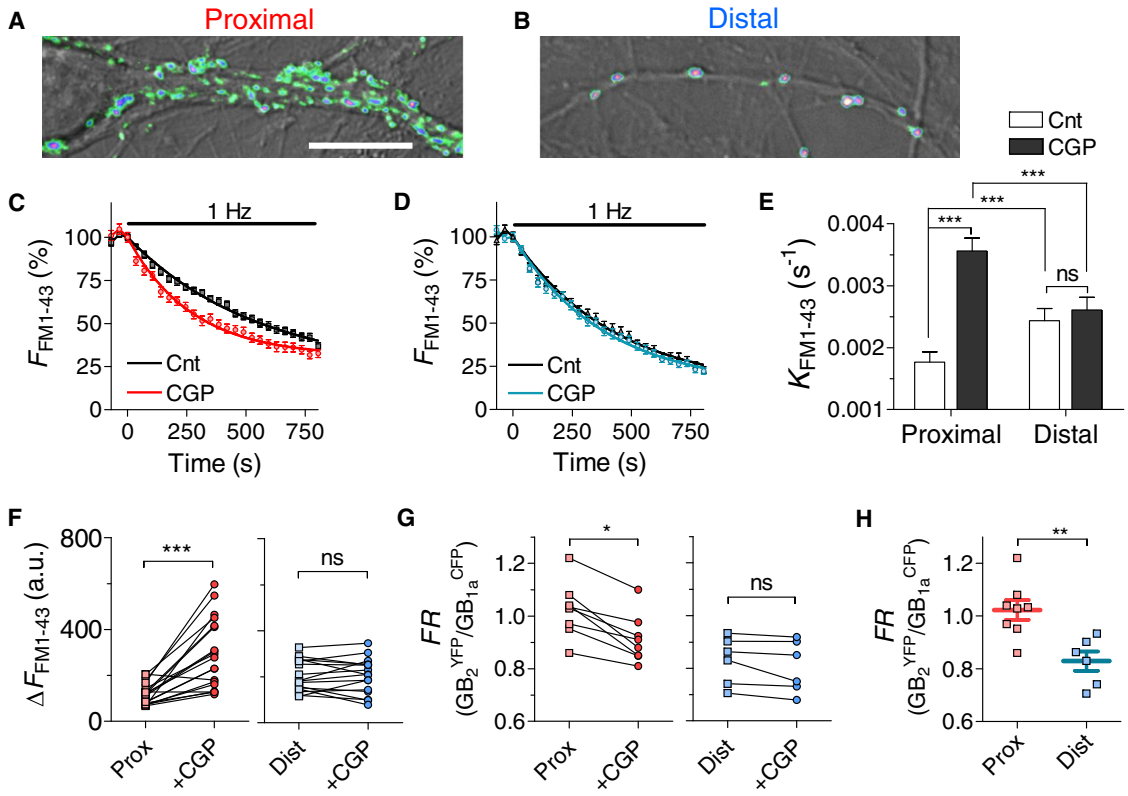

Figure 7. Differential Presynaptic GABA$_B$R Tone at Proximal versus Distal Dendrites of Pyramidal Neurons in Hippocampal Culture

(A and B) FM1-43 images of maximal stimulation (600 action potentials at 10 Hz) at proximal (A) and distal (B) dendritic branch. Fluorescence intensities (arbitrary units) are coded using a pseudocolor transformation and are merged with DIC image. Scale bar: 10 μm.

(C and D) Effect of CGP54626 (1 μM) on the destaining rate constant (*k*) during 1 Hz stimulation at proximal high-density (C) and distal low-density (D) dendrites. CGP54626 increased *k* from (1.7 ± 0.06) × 10^{-3} to (3.7 ± 0.13) × 10^{-3} s^{-1} at 67 synapses contacting proximal dendrites, but did not affect it at 71 synapses contacting distal dendrites (*k* were (2.4 ± 0.06) × 10^{-3} and (2.6 ± 0.09) × 10^{-3} s^{-1} in control and after CGP54626 application, respectively).

(E) On average (n = 4), CGP54626 mainly increased FM1-43 destaining rate in boutons at proximal dendrites ($p < 0.0001$) that display lower basal destaining rate than distal ones ($p < 0.001$).

(F) Effect of CGP54626 (1 μM) on ΔF_{FM1-43} at single boutons under miniature synaptic activity (+TTX) at proximal (left, n = 20, $p < 0.0001$) and distal (right, n = 20, $p > 0.5$) dendrites.

(G) Effect of CGP54626 (1 μM) on F_{YFP}/F_{CFP} (*FR*) at boutons expressing GB_{1a}^{CFP} and GB_2^{YFP} under miniature synaptic activity (+TTX) at proximal (left, n = 8, $p < 0.05$) and distal (right, n = 6, $p > 0.6$) dendrites.

(H) On average, *FR* between GB_{1a}^{CFP} and GB_2^{YFP} was higher at boutons contacting proximal dendrites than the distal ones (n = 6–8, $p < 0.01$) under miniature activity.

Error bars represent SEM. See also Figure S9.

To examine whether increase in the slope was due to presynaptic changes, we estimated CGP54626 effect on paired-pulse facilitation. At proximal synapses, CGP54626 reduced paired-pulse facilitation by 20% (from 211% ± 11% to 169% ± 9%, n = 7, $p < 0.01$; Figures 8C and 8D). Next, we assessed the strength of basal synaptic transmission at the most distal synapses, receiving direct input from perforant pathway of entorhinal cortex. In contrast to proximal synapses, CGP54626 significantly affected neither basal synaptic transmission (1.02 ± 0.1 versus 1.06 ± 0.07 slope for control and CGP54626, respectively, n = 9, $p > 0.8$; Figure 8E), nor synaptic facilitation (n = 9, $p > 0.7$; Figures 8F and 8G). It is worth mentioning that input-output slope was higher (0.6 ± 0.06 versus 1.02 ± 0.1), while paired-pulse facilitation was lower (142% ± 14% versus 221% ± 12%, n = 9, $p < 0.001$) at distal synapses, suggesting higher release probabilities. These results suggest differential basal GABA$_B$R activation along apical dendrites of CA1 pyramidal neurons under evoked conditions, with predominant inhibition of glutamate release at proximal synapses.

DISCUSSION

GABA$_B$R Conformational Diversity

Presynaptic GABA$_B$ receptors mediate GABA-dependent inhibition of glutamate release, impacting plasticity of hippocampal synapses and hippocampus-dependent memory function (Vigot et al., 2006). Whether presynaptic GABA$_B$Rs are activated under basal synaptic activity and impact the probability of neurotransmitter release has been unclear. To explore GABA$_B$R activation at individual hippocampal boutons, we took advantage of the

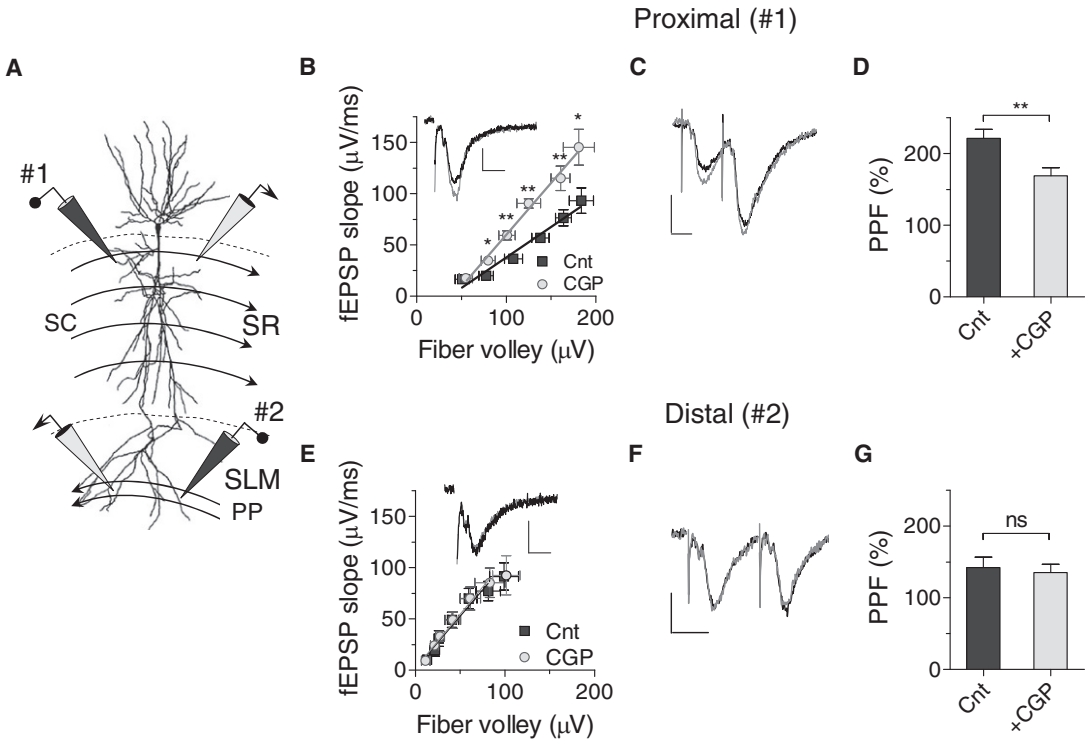

Figure 8. Differential Basal GABA$_B$R Activation at Proximal versus Distal CA1 Synapses in Hippocampal Slices

(A) Experimental set-up and CA1 organization. For recordings at proximal apical CA1 dendrites in stratum radiatum (SR), the stimulating electrode at Schaffer collateral (SC) input was placed near cell bodies ~200 μm from the recording electrode. For recording at the most distal dendrites in stratum lacunosum moleculare (SLM), the stimulating electrode at perforant path (PP) was placed ~200 μm from the recording electrode.

(B and E) Effect of 10 μM CGP54626 on input-output relationship between the amplitude of fiber volley and the slope of fEPSP for gradually increasing stimulation intensities at proximal (B, n = 5, $p < 0.01$) versus distal (E, n = 9, $p > 0.8$) synapses. Inserts: representative recordings of fEPSPs before (black) and 10 min after (gray) application of CGP54626.

(C and F) Representative recordings of paired-pulse facilitation of fEPSPs (2 action potentials; interspike interval, 20 ms; interpair interval, 30 s) before (black) and 10 min after (gray) application of CGP54626 at proximal (C) versus distal (F) synapses.

(D and G) Paired-pulse facilitation (PPF) of fEPSPs, normalized to the first peak at proximal (D) and distal (G) synapses. CGP54626 reduced PPF at proximal synapses (n = 7, $p < 0.01$), but did not affect it at distal ones (n = 9, $p > 0.7$). Note reduction in the initial PPF at distal synapses ($p < 0.001$).

Scale bars: (B, C, E, and F) 0.1 mV, 10 ms. Error bars represent SEM.

selective targeting of GB$_{1a}$ to presynaptic boutons (Vigot et al., 2006) and integrated two types of highly sensitive optical reporters, a FRET-based detector of intermolecular associations between GB$_{1a}$ and GB$_2$ receptor subunits, and FM dye-based tracking of synaptic vesicle release. We discovered an inter-synapse variability of GB$_{1a}$/GB$_2$ activity that correlates with variations in basal levels of GABA. The basal activation of GABA$_B$Rs was dendrite specific and homeostatically regulated by ongoing neuronal activity. These findings demonstrate a critical link between GABA$_B$R heterodimer conformational dynamics and local regulation of release probability at hippocampal synapses.

A prominent feature of the FRET signal detected between GB$_{1a}$ and GB$_2$ subunits is the high intersynapse heterogeneity that occurs under basal synaptic activity. Two potential sources of FRET variability may be considered: a biological one due to differences in the local [GABA]$_o$ near individual synaptic contacts and/or in the number of presynaptic GABA$_B$Rs or a methodological one due to instrumentation variability or nonspecific associations. The latter seems unlikely since negative controls did not reveal specific FRET. On the other hand, several experiments support the explanation of variations in basal [GABA]$_o$ as a major determinant of FRET variability. The variability in FRET efficiency decreased significantly with inhibiting SNARE-mediated synaptic vesicle exocytosis and interfering with binding of ambient GABA to the receptor with a selective GABA$_B$R antagonist. Furthermore, because [GABA]$_o$ depends on the balance of GABA release, up-take and diffusion, we examined the influence of these parameters on heterogeneity of FRET signals. Increasing [GABA]$_o$ by inhibiting GABA up-take resulted in ~2-fold reduction of intersynapse GB$_{1a}$/GB$_2$ FRET variability and a higher mean E_{mini} (Figure 2D), while addition of a saturating concentration of baclofen reduced variability by ~5-fold and increased the mean E_{mini} (Figure 2C). Moreover, stronger basal GABA$_B$R activation was detected at proximal thick dendrites (Figures 7 and 8). Given the higher synapse density and larger ratio of inhibitory to excitatory synapses at proximal versus distal dendrites (Figure S9), diffusion distance from inhibitory to excitatory boutons might be a significant determinant of local [GABA]$_o$ in our

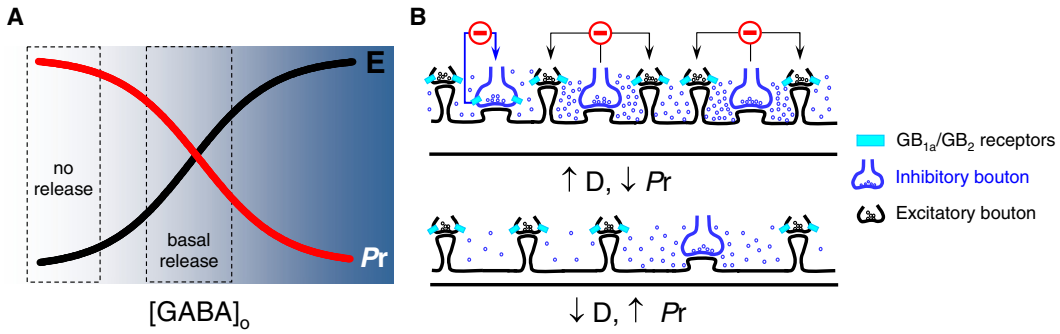

Figure 9. Illustration of the GABA$_B$R Activation at Presynaptic Boutons as Function of [GABA]$_o$

(A) [GABA]$_o$ depends on the level of presynaptic activity coded by white-blue scale. In the absence of synaptic activity (white background), GB$_{1a}$ and GB$_2$ subunits are closely associated (FRET efficiency, solid black line), while intersynapse variability of these associations (dashed black line) is low. Increase in [GABA]$_o$ under quantal transmitter release (light blue background), enhances GB$_{1a}$/GB$_2$ associations and increases their intersynapse variability, promoting GB$_{1a}$R-mediated inhibition of vesicle release (solid red line).

(B) Dendrite-specific GABA$_B$R-mediated tonic inhibition of basal vesicle release. At highly innervated proximal dendrites, GABA activates GB$_{1a}$/GB$_2$ heteroreceptors, resulting in inhibition of glutamate release and reduction in *Pr* (upper panel). A low fraction of inhibitory synapses expressing GB$_{1a}$/GB$_2$ autoreceptors trigger autoinhibition of GABA release, resulting in reduction of basal [GABA]$_o$ at neighboring excitatory synapses. At distal dendritic branches with lower synapse density, [GABA]$_o$ near glutamatergic boutons is insufficient to activate GB$_{1a}$/GB$_2$ receptors, leaving intrinsic *Pr* unaltered and, therefore, higher than at proximal branches. Excitatory synapses (black), Inhibitory synapses (blue), GABA (blue circles), GB$_{1a}$/GB$_2$ receptors (turquoise rectangle), GABA$_B$R-mediated autoinhibition of GABA release (blue arrows), GABA$_B$R-mediated inhibition of glutamate release (black arrows).

experiments. Moreover, activation of GB$_{1a}$/GB$_2$ autoreceptors at a fraction of GABAergic neurons (Figure 3) triggers negative feedback loop, inhibiting GABA release and, therefore, contributing to spatial differences in [GABA]$_o$ (Figure 9B). Collectively, these data suggest that differences in the local [GABA]$_o$ near synaptic contacts, but not in the assembly of GB$_{1a}$/GB$_2$ receptor heterodimers, is the major determinant of the FRET variability. Differences in the expression levels of endogenous GB$_{1a}$/GB$_2$ receptors at individual synapses may provide an additional element of variability in vivo.

How does the synapse-specific GB$_{1a}^{CFP}$/GB$_2^{YFP}$ FRET efficiency relate to receptor activation? The FRET efficiency is determined by the proximity and orientation of the CFP and YFP fluorophores. Notably, the mean E_{mini} in the presence of GABA$_B$R antagonist is low but significantly higher than background. This result is consistent with the known formation of an obligate heterodimer (Jones et al., 1998; Kaupmann et al., 1998; White et al., 1998). The increase in mean E_{mini} with agonist suggests the GABA$_B$R undergoes a conformational change, bringing the two fluorophores closer (or into a more favorable orientation). Remarkably, the EC$_{50}$ for FRET superimposes with the IC$_{50}$ for baclofen-dependent inhibition of presynaptic Ca^{2+} transients and of vesicle release. Previous spectroscopic FRET studies with CFP/YFP tagged G-proteins also found overlap in the EC$_{50}$ for G protein activation and FRET. The variable E_{mini} that is measured under basal synaptic activity likely reflects different activation states of the GABA$_B$ heterodimer. Nikolaev et al. (2006) examined the change in FRET with tagged α2A adrenergic receptor and different agonists and found the rate of receptor activation correlated with the ability of agonists to stabilize different receptor conformational changes (Nikolaev et al., 2006). Similarly, local [GABA]$_o$ might affect the degree of FRET between closely associated molecular pairs. In this case, activation of the GB$_{1a}$/GB$_2$ heterodimer occurs through series of conformational intermediates, suggesting general conformational flexibility similarly to adrenoreceptors (Kobilka and Deupi, 2007). Irrespective of the exact activation mechanism, our data suggest a partial GABA$_B$R activation by ambient GABA during basal synaptic activity. Thus, C terminally tagged GB$_{1a}$/GB$_2$ engineered FRET pair constitutes highly sensitive sensor for receptor activation by endogenous [GABA]$_o$.

Functional Diversity of GABA$_B$R Tone

Heterogeneity of release probability among synapses appears to be a universal property of synaptic transmission in a wide range of species (Atwood and Karunanithi, 2002). In hippocampal cultures and slices, highly variable *Pr* have been recorded utilizing electrophysiological and optical tools (Branco et al., 2008; Dobrunz and Stevens, 1997; Murthy et al., 1997; Rosenmund et al., 1993; Slutsky et al., 2004). The origin of this variability, although central to our understanding of synaptic transmission and plasticity, is not fully understood. While various morphological correlates of *Pr* have been proposed (Schikorski and Stevens, 1997), molecular mechanisms underlying functional diversity of presynaptic boutons remain obscure.

Our study suggests that the level of basal activation of presynaptic GABA$_B$Rs regulates *Pr* of individual hippocampal boutons, thus impacting functional presynaptic variability. Such a potential regulatory mechanism of intersynapse *Pr* variability was explored previously, but a uniform reduction in vesicle exocytosis by baclofen was observed across individual boutons (Isaacson and Hille, 1997). While our results confirm a homogeneous nature of baclofen-induced presynaptic inhibition (Figure 4E), we observed a remarkable variability in the positive effect of GABA$_B$R antagonist on basal presynaptic activity. An inverse correlation between basal presynaptic strength and the GB$_{1a}$/GB$_2$ conformational state at the level of individual boutons (Figure 5H) suggests that the probability of glutamate

release can be regulated through synapse-specific fine-tuning of the $GABA_BR$ activation. Based on these data, following scenario of endogenous receptor activation can be proposed (Figure 9A). During periods of synaptic inactivity which can occur before synapse maturation or as a consequence of experience-dependent synaptic depression at GABAergic boutons, local $[GABA]_o$ approximates its lowest boundary. As a result, GB_{1a}/GB_2 heterodimers at neighboring glutamatergic boutons switch to inactive conformation, blocking the $GABA_BR$-mediated signaling cascade and, consequently, leaving intrinsic probability of glutamate release unaltered. Increase in ambient $[GABA]_o$ during basal activity strengthens GB_{1a}/GB_2 associations by variable degree at glutamatergic synapses, resulting in nonuniform inhibition of glutamate release. Synchronous activation of multiple inhibitory boutons should increase local $[GABA]_o$ and might further strengthen GB_{1a}/GB_2 associations with concurrent decrease in glutamate release.

Homeostatic Regulation of $GABA_BR$ Tone

Homeostatic regulation of synaptic strength represents a basic mechanism of neuronal adaptation to chronic changes in ongoing activity levels. There is a wide repertoire of synaptic modifications at both sides of the synaptic cleft that enable neuronal homeostasis. At the presynaptic side of hippocampal synapses, strong evidence exists on augmentation of release probabilities as a homeostatic response to prolong synaptic disuse (Branco et al., 2008; Murthy et al., 2001; Thiagarajan et al., 2005). Functionally, activity-dependent presynaptic homeostasis, in contrast to the postsynaptic one, may profoundly impact short-term synaptic dynamics by altering the filtering properties of synapses. However, molecular mechanisms underlying presynaptic adaptation remain largely unknown. Our data propose reduction in the extent and variability of the $GABA_BR$ tone as a homeostatic mechanism underlying inactivity-induced increase in release probabilities and reduction in release heterogeneity (Branco et al., 2008). As activity blockade did not trigger changes in the GB_{1a}/GB_2 receptor assembly, expression level and responsiveness to agonist, we conclude that reduction in the ambient $[GABA]_o$ might cause the lost of tonic $GABA_BR$ activation. Indeed, inactivity has been demonstrated to induce reduction in the amount of GABA released by individual vesicles (De Gois et al., 2005; Hartman et al., 2006) that should reduce the ambient $[GABA]_o$. Alternatively, prolong synaptic disuse might trigger upregulation of GAT-1 GABA transporter. But, the observed lack of changes in presynaptic responsiveness to GABA transporter blocker following activity blockade (Figures 6E and 6F) makes this possibility less likely. Given a predominant localization of GB_{1a}/GB_2 receptors at excitatory boutons (Vigot et al., 2006), homeostatic regulation of the $GABA_BR$ tone may preferentially adjust release probabilities of glutamatergic vesicles. Interestingly, inhibitory neurons expressing CB_1Rs have been recently shown to increase their release probabilities in response to chronic inactivity through reduction in endocannabinoid tone (Kim and Alger, 2010). Future studies are warranted to examine whether tuning basal activation of high-affinity presynaptic GPCRs represents a general mechanism of presynaptic homeostasis in other central synapses.

Dendrite-Specific Scaling of the $GABA_BR$ Tone

While high heterogeneity of release probability and Ca^{2+} flux dynamics have been observed at boutons along axons (Koester and Sakmann, 2000; Murthy et al., 1997), release properties of neighboring synapses tend to be correlated at spatially restricted subdomains of dendritic tree (Branco et al., 2008; Murthy et al., 1997). Postsynaptic target specificity of transmitter release suggests that differential retrograde messenger signaling (Davis et al., 1998), and local postsynaptic depolarization levels (Branco et al., 2008) might contribute to presynaptic differentiation. Our results demonstrate that $GABA_BR$-mediated presynaptic inhibition is dendrite specific, being more pronounced at proximal than at distal dendritic branches of CA1 hippocampal neurons in hippocampal cultures and acute slices. Our single-synapse analysis of presynaptic activity in cultures suggests different synaptic configuration of proximal versus the distal dendrites (Figure 9B): proximal branches display higher ratio of inhibitory-to-excitatory synapses, higher total synapse density and lower *Pr* due to higher extent of presynaptic $GABA_BR$ tone. In slices, the most proximal SC synapses along apical dendrites of CA1 pyramidal cells, with higher inhibitory-to-excitatory synapse ratio (Megías et al., 2001), displayed higher paired-pulse facilitation, lower input-output slope, and higher $GABA_BR$ activation under low-frequency stimulation than the most distal perforant synapses. At first glance, our results seem to differ from the data by Ahmed and Siegelbaum (2009), suggesting higher *Pr* and lower paired-pulse ratio at Schaffer collateral than at perforant CA1 synapses. This discrepancy can be attributed to differences in the experimental design. Ahmed and Siegelbaum performed recordings from medial Shaffer collateral synapses while our study focused on proximal synapses. In addition, their ACSF included $GABA_BR$ and $GABA_AR$ blockers, and $[Ca^{2+}]_o$ twice as high as in our study, making the direct comparison problematic.

Local fine-tuning of presynaptic $GABA_BR$ tone may be involved in synaptic scaling along dendritic compartment, leading to homeostasis of basal synaptic activity through a negative correlation between the number of functional boutons and unitary synaptic strength (Liu and Tsien, 1995) or its presynaptic determinant, *Pr* (Branco et al., 2008). Moreover, differential presynaptic $GABA_BR$ tone along dendritic tree might enable higher dynamic range of synapses at highly innervated dendrites during temporospatially correlated synaptic activity, local inhibition-excitation balance (Liu, 2004), and normalization of synaptic inputs (Magee and Cook, 2000) in hippocampal networks. It remains to be seen whether tuning of GB_{1a}/GB_2 heterodimer conformation emerges as a possible molecular basis for feedback regulation of transmitter release and its plasticity by local dendritic activity in vivo.

EXPERIMENTAL PROCEDURES

Hippocampal Cell Culture

Primary cultures of CA3-CA1 hippocampal neurons were prepared from newborn Wistar rats on postnatal days 0–2, as described (Slutsky et al., 2004). The experiments were performed in 12–18 DIV cultures (except those performed in 4–5 DIV young neurons as mentioned in the text). All animal experiments were approved by the Tel Aviv University Committee on Animal Care.

Confocal Imaging

Hippocampal neurons were imaged using a Zeiss LSM510 META and FV1000 spectral confocal microscopes. The experiments were conducted at room temperature in extracellular Tyrode solution that contained (in mM): NaCl, 145; KCl, 3; glucose, 15; HEPES, 10; $MgCl_2$, 1.2; $CaCl_2$, 1.2 (pH adjusted to 7.4 with NaOH). To isolate miniature synaptic activity, TTX (1 μM) has been added to extracellular solution. FRET imaging was carried out as above. For spectral analysis, CFP was excited at 405 nm (Zeiss) or at 442 nm (Olympus) and fluorescence emission was measured between 400 and 700 nm, with a 10 nm λ step size. In order to reduce phototoxicity and photobleaching, most of the FRET experiments were performed using a narrowed emission spectrum (470–550 nm, 20 nm λ step size) composed of CFP peak (486 ± 10 nm) and a YFP peak (534 ± 10 nm) containing YFP emission due to FRET, direct YFP excitation at 405 nm, and CFP emission tail. YFP was imaged and specifically photobleached at 514 nm (excitation, 100% laser power, 30 ms duration) and 534 ± 5 nm (emission). Notably, photobleaching at 514 nm was specific and did not significantly affect YFP signal at neighboring boutons (Figure S1B). YFP fluorescence recovery after photobleaching was ~18% and developed within ~40 s following photobleaching (Figures S1C and S1D). Thus, images of CFP were captured within ~30 s from photobleaching. We verified that this procedure did not affect functionality of presynaptic boutons (Figure S1E).

The emission spectral properties of FM4-64 allow simultaneous imaging with CFP and YFP fluorophores (Figure S1F). Images were 512 × 512 pixels, with a pixel width of 92–110 nm. Z stacks were collected from 3–4 μm optical slice, at 0.6–0.8 μm steps.

Calculation of FRET Efficiency

Donor dequenching due to the desensitized acceptor was measured from CFP emission (486 ± 10 nm) before and after the acceptor photobleaching. FRET efficiency, E, was then calculated using the equation $E = 1 - I_{DA}/I_D$, where I_{DA} is the peak of donor emission in the presence of the acceptor and I_D is the peak after acceptor photobleaching (Riven et al., 2003). Detection of CFP/YFP signals has been done using custom-written scripts in MATLAB (see Supplemental Experimental Procedures).

FM-Based Imaging

Activity-dependent FM1-43 and FM4-64 styryl dye have been used to detect functional boutons. FM loading and unloading were done using protocols described previously (Abramov et al., 2009, and in Supplemental Experimental Procedures). The fluorescence of individual synapses was determined from the difference between images obtained after staining and after destining (ΔF). To stain all the functional boutons capable of vesicle recycling, we used maximal stimulation protocol: 600 action potentials at a rate of 10 Hz or high KCl solution (50 mM, 1 min). To estimate vesicle recycling/release during low-frequency stimulation, we quantified (1) ΔF signal for staining by 30 action potentials at a rate of 0.2 Hz stimulation, (2) FM destaining rate during 1 Hz stimulation following staining of boutons by maximal stimulation. For FM^+ puncta detection, ΔF images have been analyzed (only the puncta exhibiting ≥90% destining were subjected to analysis). For ΔF analysis, see Supplemental Experimental Procedures.

Detecting Presynaptic Calcium Transients

Fluorescent calcium indicator Calcium Green 488 BAPTA-1 AM was dissolved in DMSO to yield a concentration of 1 mM. For cell loading, cultures were incubated at 37°C for 30 min with 3 μM of this solution diluted in a standard extracellular solution. Imaging was performed using FV300 ad FV1000 Olympus confocal microscopes, under 488 nm (excitation) and 510–570 nm (emission), using 500 Hz line scanning.

Electrophysiology in Acute Hippocampal Slices

Coronal hippocampal slices (400 μm) from 5- to 7-week-old Wistar rats were prepared using standard procedures as described (Abramov et al., 2009; see Supplemental Experimental Procedures). The ACSF contained, in mM: NaCl, 125; KCl, 2.5; $CaCl_2$, 1.2; $MgCl_2$, 1.2; $NaHCO_3$, 25; NaH_2PO_4, 1.25; glucose, 25. Extracellular fEPSPs were recorded at room temperature with a glass pipette containing ACSF (1–2 MΩ) from proximal synapses in the CA1 stratum radiatum or distal synapses in stratum lacunosum moleculare using a MultiClamp700A amplifier (Molecular Devices). Stimulation of the SC or PP pathway was delivered through a glass suction electrode (10–20 μm tip) filled with ACSF. fEPSPs were analyzed by pClamp10 software (Molecular Devices).

Statistical Analysis

All error bars represent standard error. For experiments in cultures, n is designated for the number of boutons and N for the number of imaged neurons (or number of experiments for population FM analysis). All the experiments were repeated at least in 3 different batches of cultures. For slice experiments (Figure 8), n marks the number of slices. One-way ANOWA Kruskal-Wallis nonparametric test and Student's t tests were used. Nonparametric Spearman test was used for correlation analysis.

SUPPLEMENTAL INFORMATION

Supplemental Information includes nine figures and Supplemental Experimental Procedures and can be found with this article online at doi:10.1016/j.neuron.2010.06.022.

ACKNOWLEDGMENTS

We thank Dr. Bernhard Bettler for critical comments on the manuscript; Dr. Nathan Dascal and Dr. Bernard Attali for discussions; Dr. Eitan Reuveny for providing $TNFR_2^{YFP}$, $G\beta_1^{YFP}$ and $G\gamma_2^{CFP}$ cDNAs; Dr. Daniel Gitler for Syn_{1a}^{CFP} and Hilla Fogel for the help with image processing algorithms. This work was supported by Binational Science Foundation (I.S. and P.A.S., grant No. 2007199) and Israel Science Foundation (I.S., grants No. 993/08 and 170/08).

Accepted: June 14, 2010
Published: July 28, 2010

REFERENCES

Abramov, E., Dolev, I., Fogel, H., Ciccotosto, G.D., Ruff, E., and Slutsky, I. (2009). Amyloid-beta as a positive endogenous regulator of release probability at hippocampal synapses. Nat. Neurosci. *12*, 1567–1576.

Ahmed, M.S., and Siegelbaum, S.A. (2009). Recruitment of N-Type Ca(2+) channels during LTP enhances low release efficacy of hippocampal CA1 perforant path synapses. Neuron *63*, 372–385.

Atwood, H.L., and Karunanithi, S. (2002). Diversification of synaptic strength: presynaptic elements. Nat. Rev. Neurosci. *3*, 497–516.

Bettler, B., Kaupmann, K., Mosbacher, J., and Gassmann, M. (2004). Molecular structure and physiological functions of GABA(B) receptors. Physiol. Rev. *84*, 835–867.

Branco, T., Staras, K., Darcy, K.J., and Goda, Y. (2008). Local dendritic activity sets release probability at hippocampal synapses. Neuron *59*, 475–485.

Davis, G.W., DiAntonio, A., Petersen, S.A., and Goodman, C.S. (1998). Postsynaptic PKA controls quantal size and reveals a retrograde signal that regulates presynaptic transmitter release in *Drosophila*. Neuron *20*, 305–315.

De Gois, S., Schäfer, M.K.H., Defamie, N., Chen, C., Ricci, A., Weihe, E., Varoqui, H., and Erickson, J.D. (2005). Homeostatic scaling of vesicular glutamate and GABA transporter expression in rat neocortical circuits. J. Neurosci. *25*, 7121–7133.

Dobrunz, L.E., and Stevens, C.F. (1997). Heterogeneity of release probability, facilitation, and depletion at central synapses. Neuron *18*, 995–1008.

Fowler, C.E., Aryal, P., Suen, K.F., and Slesinger, P.A. (2007). Evidence for association of GABA(B) receptors with Kir3 channels and regulators of G protein signalling (RGS4) proteins. J. Physiol. *580*, 51–65.

Hartman, K.N., Pal, S.K., Burrone, J., and Murthy, V.N. (2006). Activity-dependent regulation of inhibitory synaptic transmission in hippocampal neurons. Nat. Neurosci. *9*, 642–649.

Isaacson, J.S., and Hille, B. (1997). GABA(B)-mediated presynaptic inhibition of excitatory transmission and synaptic vesicle dynamics in cultured hippocampal neurons. Neuron *18*, 143–152.

Isaacson, J.S., Solís, J.M., and Nicoll, R.A. (1993). Local and diffuse synaptic actions of GABA in the hippocampus. Neuron *10*, 165–175.

Jensen, K., Chiu, C.-S., Sokolova, I., Lester, H.A., and Mody, I. (2003). GABA transporter-1 (GAT1)-deficient mice: differential tonic activation of GABAA versus GABAB receptors in the hippocampus. J. Neurophysiol. *90*, 2690–2701.

Jones, K.A., Borowsky, B., Tamm, J.A., Craig, D.A., Durkin, M.M., Dai, M., Yao, W.J., Johnson, M., Gunwaldsen, C., Huang, L.Y., et al. (1998). GABA(B) receptors function as a heteromeric assembly of the subunits GABA(B)R1 and GABA(B)R2. Nature *396*, 674–679.

Kaupmann, K., Malitschek, B., Schuler, V., Heid, J., Froestl, W., Beck, P., Mosbacher, J., Bischoff, S., Kulik, A., Shigemoto, R., et al. (1998). GABA(B)-receptor subtypes assemble into functional heteromeric complexes. Nature *396*, 683–687.

Kim, J., and Alger, B.E. (2010). Reduction in endocannabinoid tone is a homeostatic mechanism for specific inhibitory synapses. Nat. Neurosci. *13*, 592–600.

Kobilka, B.K., and Deupi, X. (2007). Conformational complexity of G-protein-coupled receptors. Trends Pharmacol. Sci. *28*, 397–406.

Koester, H.J., and Sakmann, B. (2000). Calcium dynamics associated with action potentials in single nerve terminals of pyramidal cells in layer 2/3 of the young rat neocortex. J. Physiol. *529*, 625–646.

Liu, G. (2004). Local structural balance and functional interaction of excitatory and inhibitory synapses in hippocampal dendrites. Nat. Neurosci. *7*, 373–379.

Liu, G., and Tsien, R.W. (1995). Properties of synaptic transmission at single hippocampal synaptic boutons. Nature *375*, 404–408.

Magee, J.C., and Cook, E.P. (2000). Somatic EPSP amplitude is independent of synapse location in hippocampal pyramidal neurons. Nat. Neurosci. *3*, 895–903.

Malitschek, B., Rüegg, D., Heid, J., Kaupmann, K., Bittiger, H., Fröstl, W., Bettler, B., and Kuhn, R. (1998). Developmental changes of agonist affinity at GABABR1 receptor variants in rat brain. Mol. Cell. Neurosci. *12*, 56–64.

Matsushita, S., Nakata, H., Kubo, Y., and Tateyama, M. (2010). Ligand-induced rearrangements of the GABA(B) receptor revealed by fluorescence resonance energy transfer. J. Biol. Chem. *285*, 10291–10299.

Megías, M., Emri, Z., Freund, T.F., and Gulyás, A.I. (2001). Total number and distribution of inhibitory and excitatory synapses on hippocampal CA1 pyramidal cells. Neuroscience *102*, 527–540.

Murthy, V.N., Sejnowski, T.J., and Stevens, C.F. (1997). Heterogeneous release properties of visualized individual hippocampal synapses. Neuron *18*, 599–612.

Murthy, V.N., Schikorski, T., Stevens, C.F., and Zhu, Y. (2001). Inactivity produces increases in neurotransmitter release and synapse size. Neuron *32*, 673–682.

Nikolaev, V.O., Hoffmann, C., Bünemann, M., Lohse, M.J., and Vilardaga, J.P. (2006). Molecular basis of partial agonism at the neurotransmitter alpha2A-adrenergic receptor and Gi-protein heterotrimer. J. Biol. Chem. *281*, 24506–24511.

Riven, I., Kalmanzon, E., Segev, L., and Reuveny, E. (2003). Conformational rearrangements associated with the gating of the G protein-coupled potassium channel revealed by FRET microscopy. Neuron *38*, 225–235.

Rosenmund, C., Clements, J.D., and Westbrook, G.L. (1993). Nonuniform probability of glutamate release at a hippocampal synapse. Science *262*, 754–757.

Scanziani, M. (2000). GABA spillover activates postsynaptic GABA(B) receptors to control rhythmic hippocampal activity. Neuron *25*, 673–681.

Schikorski, T., and Stevens, C.F. (1997). Quantitative ultrastructural analysis of hippocampal excitatory synapses. J. Neurosci. *17*, 5858–5867.

Slutsky, I., Sadeghpour, S., Li, B., and Liu, G. (2004). Enhancement of synaptic plasticity through chronically reduced Ca2+ flux during uncorrelated activity. Neuron *44*, 835–849.

Thiagarajan, T.C., Lindskog, M., and Tsien, R.W. (2005). Adaptation to synaptic inactivity in hippocampal neurons. Neuron *47*, 725–737.

Vigot, R., Barbieri, S., Bräuner-Osborne, H., Turecek, R., Shigemoto, R., Zhang, Y.P., Luján, R., Jacobson, L.H., Biermann, B., Fritschy, J.M., et al. (2006). Differential compartmentalization and distinct functions of GABAB receptor variants. Neuron *50*, 589–601.

White, J.H., Wise, A., Main, M.J., Green, A., Fraser, N.J., Disney, G.H., Barnes, A.A., Emson, P., Foord, S.M., and Marshall, F.H. (1998). Heterodimerization is required for the formation of a functional GABA(B) receptor. Nature *396*, 679–682.

Wu, L.G., and Saggau, P. (1995). GABAB receptor-mediated presynaptic inhibition in guinea-pig hippocampus is caused by reduction of presynaptic Ca2+ influx. J. Physiol. *485*, 649–657.

Wu, L.G., and Saggau, P. (1997). Presynaptic inhibition of elicited neurotransmitter release. Trends Neurosci. *20*, 204–212.